Low Computation Acoustic Emissions Structural Health Monitoring Through Analog Signal Pre-Processing

Rune Schlanbusch[1], Eric Bechhoefer[2], and Thomas J. J. Meyer[3]

[1,3] *Teknova, Kristiansand, Norway*
rune.schlanbusch.2008@ieee.org
thomas.meyer@teknova.no

[2] *GPMS Inc, Cornwall, VT, USA*
eric@gpms-vt.com

ABSTRACT

In this research an innovative acoustic emission sensing system has been developed intended for structural fatigue crack monitoring. The innovation lies in analog pre-processing of the detected acoustic emissions for signal enveloping, thus relying on cheap high bandwidth components. The technique is based on heterodyning the amplified acoustic emission signal with a carrier signal of a chosen frequency. Next, the signal is filtered and the signal envelope is obtained by phase shifting the signal by $\pi/2$ creating an analytic signal that is digitally sampled. This results in need of low sampling rate digital acquisition equipment giving relatively small amounts of data to be processed and stored, considerably reducing the system cost. This is particularly suitable for applications involving large or complex structures to be monitored, where a multitude of sensors are needed. The system was built and tested on aluminum test coupons during tension-tension fatigue. The envelope signal is filtered for background noise through thresholding based on statistical knowledge of the noise distribution. The accumulation of acoustic activity shows promising results with an early period of high acoustic activity during settling of the material that asymptotically converges at a certain level. At the next stage, there is no activity until a certain point is reached where a sudden ramp up of AE is detected close to the end of the experiment. Through extensometer measurement, the change in coupon length at this point in time strongly indicates that the ramp up of AE activity is due to crack initiation and propagation.

1. INTRODUCTION

Acoustic emissions (AE) are the stress waves produced by a sudden internal stress redistribution of material caused by the changes in the internal structure of the material. Various causes of these changes include crack initiation and growth, crack opening and closure or pitting, in various typical system components such as bearing races and gears, and materials such as steel, aluminum, concrete, fiberglass and various composites. There are several examples of real world application utilizing the AE technique for condition monitoring including steel wire rope monitoring of suspension bridges, integrity monitoring of concrete structures such as bridges, integrity monitoring of pressure vessels, rock stability for pre-detecting rock failure (avalanche), damage monitoring of aircraft structure and rocket motor cases, and evaluation of corrosion damage during tank bottom testing, to name a few (Mizutani, 2016).

Fatigue crack propagation monitoring and characterization has been widely studied (Lindley, Palmer, & Richards, 1978; Berkovits & Fang, 1995; Roberts & Talebzadeh, 2003) for a large variety of alloys and geometries. Studies include analysis of crack initiation, emissions at varying stages of the tension cycle to differentiate between crack closing and propagation, and for estimating future crack propagation. The latter is often associated with trying to fit experimentally obtained AE parameters with crack propagation models such as Paris' law.

Traditionally, AE data is sampled at high sampling rate due to relative high AE frequencies in the range of 100 to 1000 kHz, leading to sample rates in the range of 1 to 10 Msps. This again leads to a severe computational burden for real time processing and need of huge storage capacity. For large structures with tens or even hundreds of monitoring points, the data storage and processing requirements are tremendous. To cope with these challenges, the data is often compressed into "classical" AE parameters where data without informa-

tion[1] data is rejected and each AE event is converted into a set of parameters such as duration, frequency, number of threshold crossings (counts), rise time, amplitude and energy, for ease of post processing and analysis. Note that this does not reduce the burdens of high sampling rate and pre-processing. An introduction to the history, fundamentals, parameters and analysis of AE can be found in (Grosse & Ohtsu, 2008).

To reduce the burden associated with acquiring and processing the large amount of data captured through a common AE system, analog signal processing is a viable option. Bechhoefer et al. (Bechhoefer, Qu, Zhu, & He, 2013) proposed to apply the Hilbert transform by premixing the analog signal and low pass filtration before sampling the envelope components at low sampling frequency. The technique was successfully applied for gear fault analysis. A similar technique was also utilized for bearing fault diagnostics (Van Hecke, 2015).

Analogue enveloping and filtering of the AE signal can be seen as a data compression strategy, and loss of information is inevitable. On the other hand, the important parameters for crack propagation found in literature is event rate and accumulation of events (Berkovits & Fang, 1995; Roberts & Talebzadeh, 2003). For other applications such as wire breaks due to fatigue in steel wire ropes, event amplitude and accumulated energy are important parameters (Drummond, Watson, & Acarnley, 2007). All of this information is extractable from the proposed signal processing scheme presented in this article.

In this research we have developed and built an AE sensing system that, shown through testing, is capable of detecting crack initiation and propagation at a sampling frequency of 10k samples per second (sps). It is thus suggested that the method is highly suitable for developing a low cost system for real-time monitoring of cracks. The technique first mixes an amplified AE signal with a carrier signal with predefined frequency that is chosen based on the application, to move the signal content into low frequency range, and filters out the high frequency content, i.e. heterodying. Next, still in the analog domain, the system performs the Hilbert transform on the heterodyned signal, and both the heterodyned and the Hilbert transformed signal are digitally sampled. The two channels are then merged to form the signal envelope. The background noise is then filtered out by thresholding the envelope through statistical analysis. The signal above the threshold value is the integrated and shows two regimes. The first regime is a settling phase of the material asymptotically converging towards a fixed value, i.e. the signal does not pass the statistical threshold. The next regime is located when the integrated signal again starts increasing, indicating start of the cracking process that develops until rupture. The result is cheap to implement and has shown through experiment to work well at digital sampling frequencies 1000 times lower than typical commercial systems. The system was successfully tested on aluminum test coupons during tension-tension testing. The technique clearly indicated the point of crack initiation, that also can be traced until rupture. The result was verified against extensometer data yielding perfect agreement.

[1]Signals below a predefined threshold is assumed to be background or operational noise and thus is rejected.

2. ANALOG AE SYSTEM

The main idea is that the carrier frequency of the acoustic emission is not containing the interesting information of damage, but instead the energy and number of events. Thus, the goal for the AE monitoring system is to reduce the sampling and processing requirements for on-line monitoring of structural components and thus facilitates detection of high cycle/amplitude fatigue damage.

The AE phenomenon associated with dislocation and crack propagation through plastic deformation can be estimated (Liptai, Dunegan, & Tatro, 1969). The stress driving the deformation is calculated as

$$\sigma_s = \frac{sG}{d}, \tag{1}$$

where σ_s is the deformation stress, s is the slip distance, G is the shear modulus, and d is grain boundary diameter. The energy change occurring due to the deformation is calculated as

$$\Delta E = \frac{s^2 GA}{2d} \tag{2}$$

where ΔE is the energy change associated with deformation, and A is the shear area. By combining Eqs. (1) and (2), the frequency of the slip event can be estimated as

$$\omega = \sqrt{\frac{2GA}{dm}}, \tag{3}$$

where ω is the estimated frequency of the slip event and m is the half mass of the grain estimated based on a spheric volume of steel. By plugging in numbers, (Bechhoefer et al., 2013) showed that for a polycrystalline material with grain boundary of 5×10^{-3} inch diameter experiencing a 1×10^{-3} inch slip during a strain event, i.e. the grain has about 15 grain boundaries along its circumference. Assuming a steel shear modulus of 4×10^6 psi, the resulting estimated frequency of the slip event is 0.8 MHz.

As the carrier frequency is not containing the interesting information of damage, the signal can be heterodyned by using the approximated carrier frequency. Heterodyning is a well-known signal processing technique successfully applied within the field of radio frequency (RF) communication. The demodulation is achieved by multiplying the raw AE signal with the carrier frequency, similar to amplitude modulation

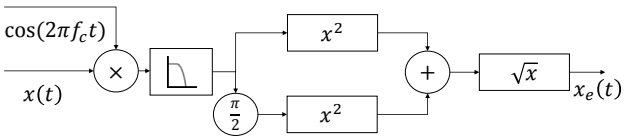

Figure 1. Schematics of analog signal processing circuit.

(AM), yielding

$$\cos(\omega t)cos(\omega_c t) = \frac{1}{2}\left[\cos((\omega-\omega_c)t) + \cos((\omega+\omega_c)t)\right] \tag{4}$$

where ω is the frequency of the recorded AE signal and ω_c is the carrier frequency. The carrier frequency can be chosen freely by using e.g. a hand held signal generator, or by low pass filtering a variable period pulse width modulation (PWM) signal. This makes it easy to adapt the system for any AE phenomenon of interest within the sensitivity frequency range of the AE sensor, which typically is the limiting component. The higher frequency image of the signal is then removed through low-pass filtering. Next, to create the envelope Hilbert transform is utilized. In frequency domain, the Hilbert transform is defined as $2X(f)$ for $f > 0$, and $X(f) = 0$ for $f < 0$. For analog implementation, the envelope can be obtained by phase shifting the base band signal by $\pi/2$ radians. Then, the base band signal and phase shifted signal are both squared, summed and square rooted. The process is illustrated in Figure 1. Such a circuit can easily be realized by using a Delta-Sigma ADC architecture, which allows changing the sample rate and effective sensor bandwidth without the use of an anti-aliasing filter network[2], which reduces the complexity of the AE sensor system.

Note that the output $x_e(t)$ contains all the necessary condition indicators (CIs) associated with classical AE including events, amplitude, rise time, duration and mean area under rectified signal envelope (MARSE).

3. AE FILTERING

For detecting the AE event, it is necessary to remove the white noise signal. The energy associated with the white noise signal can be modeled as $X = Y = N(0, \sigma)$ giving an envelope energy of

$$E(x_e) = \sqrt{(X^2 + Y^2)}. \tag{5}$$

If we assume that X and Y are normal with zero mean, the probability distribution will follow a chi distribution with second degree of freedom, also known as Rayleigh distribution. The relationship between form parameter β and variance σ for the Rayleigh distribution is given as

$$\sigma^2 = \left(2 - \frac{\pi}{2}\right)\beta^2, \tag{6}$$

and solving for β yields

$$\beta = \frac{\sigma}{\sqrt{2 - \frac{\pi}{2}}}. \tag{7}$$

The AE signal energy not associated with noise is assumed due to dislocation and should be accumulated, similar to the energy accumulation strategy as condition indicator for classical AE method. The strategy is then to choose a suitable probability of false alarm (PFA), collect a AE data series of background noise and calculate the variance. Then, the form parameter is found according to Eq. (7). A normalization parameter γ for the process is then found by applying the inverse Rayleigh cumulative distribution function (CDF) using the appropriate form parameter and PFA. An envelope gain/normalization factor can then be calculated as

$$G = \frac{\delta}{\gamma}, \tag{8}$$

where δ is a chosen threshold e.g. 1. Thus, by multiplying the enveloped signal by the normalization factor G, the signal exceeding the threshold δ is classified as AE activity from the material, while signal below δ is considered noise. The envelope time series is multiplied by the gain, and each point of the envelope crossing the threshold is assumed damage and is accumulated similar to accumulating MARSE for classical AE.

4. EXPERIMENT

In this section we describe the experiment for validating the AE system and signal filtering technique as described in Sections 2 and 3. The experiment was conducted at the machine laboratory at the University of Agder, Norway using the axial strain test machine shown in Figure 2 with a max capacity of ± 25 kN, and stable frequency up to 5 Hz. The test design was based on the guidelines given in (ISO, 2003).

The test specimens were machined in 6061-T6 aluminum based on the (ISO, 2003) standard and the following calculations. To avoid max capacity of the machine $F = 2$ kN. The number of cycles is chosen as $N = 2 \times 10^5$. The zero mean stress is then fetched from (Yahr, 1993) as $\sigma_{zm} = 64.45$ MPa. The equation of calculating stress $\sigma_{zm} = F/A$ can then be solved for area, yielding

$$A = \frac{F}{\sigma_{zm}} = \frac{2\text{ kN}}{64.45\text{ MPa}} = 3.11 \times 10^{-5}\text{ m}^2. \tag{9}$$

The stock depth is 3.18 mm, thus the width should be equal to

$$w = \frac{A}{d} = \frac{3.11 \times 10^{-5}\text{ m}^2}{3.18 \times 10^{-3}\text{ m}} = 9.78 \times 10^{-3}\text{ m}. \tag{10}$$

[2]Generally, a Delta-Sigma ADC uses oversampled input signals and a finite impulse response (FIR) filter to eliminate aliasing.

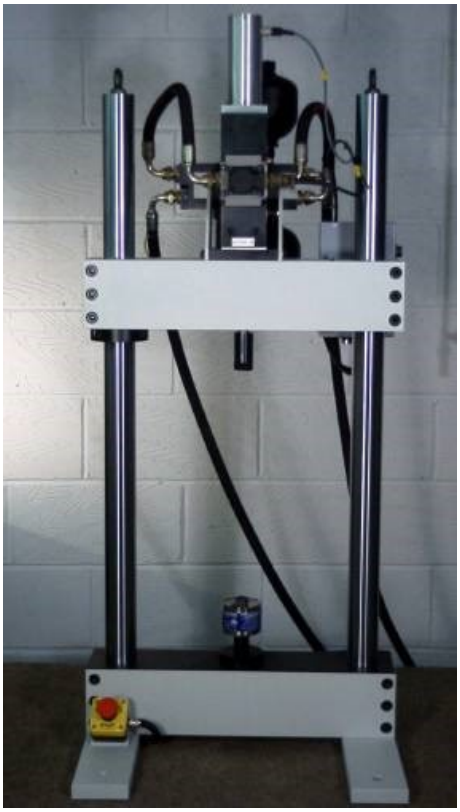

Figure 2. Axial strain test machine.

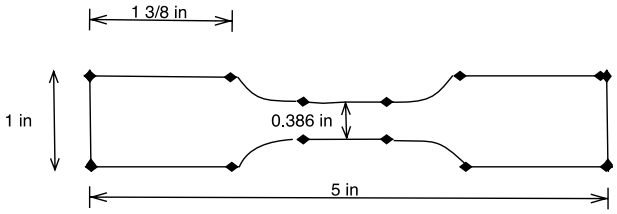

Figure 3. Design of test coupon.

The expected yield force is found by

$$F = \sigma A = 265 \times 10^6 \times 3.18 \times 10^{-3} \times 9.78 \times 10^{-3} = 8.26 \text{ kN}, \quad (11)$$

where σ is the material yield stress. A drawing of the coupon design is shown in Figure 3.

The signal processing and data acquisition system utilized can be seen in Figure 4 and the equipment description is summarized in Table 1.

The test coupons were mounted vertically in the test machine shown in Figure 5, and the AE sensor was glued to the test coupon using Loctite super glue close to the gripper. The device mounted on the center of the specimen is the extensometer, measuring elongation with high precision compared to

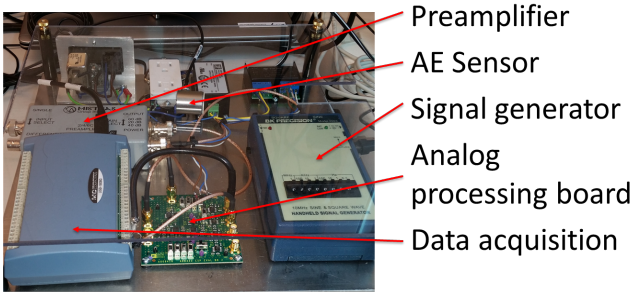

Figure 4. Analog signal processing and data acquisition.

Table 1. Analog signal processing and data acquisition equipment description.

Equipment	**Model & Description**
AE Sensor	Mistras R15a, pn# R15a, SENSOR, 150KHZ W/SMA CONN - ALPHA S
AE Sensor cable	Mistras 1232-SMA/BNC-2, pn# 1232-4001-002, SENSOR CABLE, BNC TO SMA, 2M (For Alpha sensors)
Preamplifier	Mistras 2/4/6 Type C Preamplifier, pn# 1220-5045, 2/4/6 single-ended/differential AST preamplifier with a 2/4/6 series filter (Filter Range: 100HP), powered by 28V DC through a separate BNC
Signal cable	Mistras 1234-BNC/BNC-2 m, pn# 1234-2, SIGNAL CABLE, RG-58, BNC - BNC, 2M1
Signal generator	BK Precision 10 MHz Sine/Square Wave Generator Model 3003
Analog processing board	PCB with analog heterodyne, filtering and Hilbert transform with real and imaginary parts as two separate outputs
Data acquisition	Measurement computing USB-1608G

the cylinder displacement measurement on the test machine. The DAQ was configured to sample at 10 ksps at both channels, with 400 kHz on the signal generator used for analogue mixing. The mixing frequency was chosen to be in the upper end of the sensitivity spectrum for the sensor to minimize the amount of low frequency noise, while still being within the expected frequency range of the elastic wave excited by the crack initiation and growth. For specific applications the mixing frequency should be chosen based on material type and geometry of object under monitoring. The sampling of each channel for each data point was with minimum delay in between the samplings. All coupons were measured, and found to be agreeing with the design specifications with small variations ($\sim$0.01mm). The tests were conducted based on the

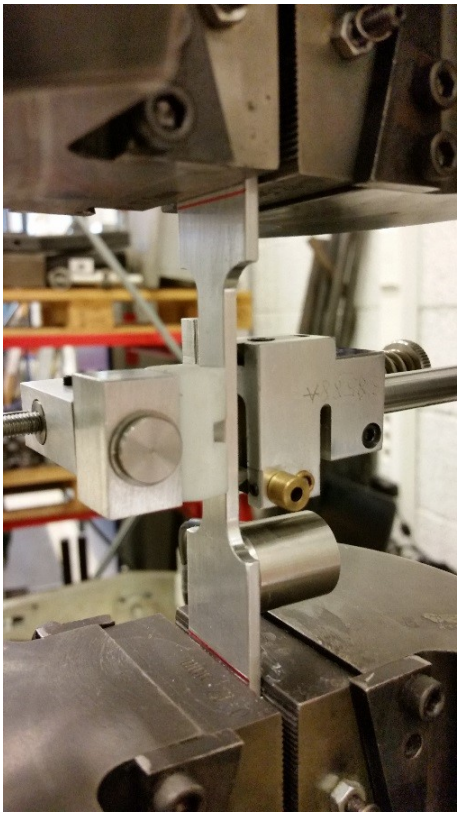

Figure 5. Test coupon mounted in tensile machine with AE sensor and extensometer attached.

stress ratio

$$R = \frac{\sigma_{min}}{\sigma_{max}} = 0.1. \quad (12)$$

From the first test, the yield strength (0.2 % elongation or "knee point") was found to be approximately 8.3 kN fitting very well with the estimation of 8.26 kN. Tensile fatigue testing requires a high number of cycles, in the range of millions, for low stress values. Due to the low cycle frequency of the machine used for testing it was decided to test at close to 100% of the tensile force, yielding approximately 35,000 cycles endurance before rupture of test coupon.

The setup was tested based on the pencil lead break test giving an envelope as showed in Figure 6 (100 samples equals 10 ms).

By integrating the envelope over time the curve is almost linear due to noise, as seen in Figure 7. One characteristic can be noted though, which is that the integration curve is somewhat steeper during the first 1500 seconds. This is due to the fact that metals in fatigue experiments tends to settle for some time due to imperfect structure, adapting to impurities etc. causing dislocations and thus AE activity. Due to large amount of noise accumulated, giving a very wide range along the y-axis, it can not easily be seen that the coupon ruptured after 7200 seconds. It can be noticed that after the rupture,

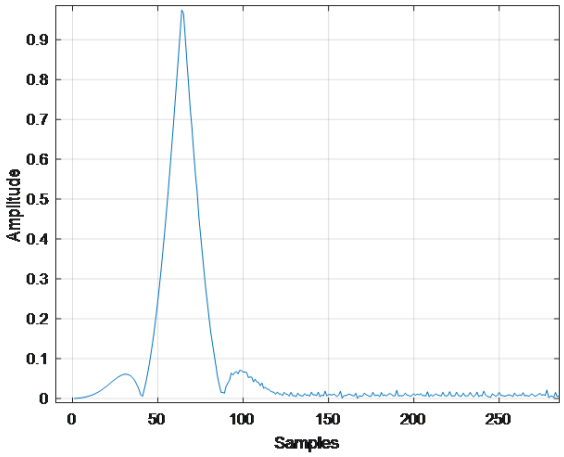

Figure 6. Envelope signal from pencil lead test.

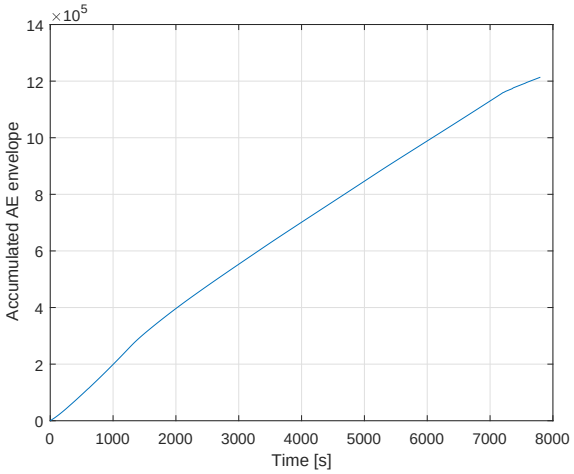

Figure 7. Time integration of AE envelope signal.

the accumulated signal curve is less steep after this point due to less noise accumulated as the machine was stopped.

Next, the filtering algorithm described in Section 3 was applied by fitting the pdf over the first 10 seconds of data from the envelope data series. The resulting Rayleigh distribution reasonably well fits the recorded data, as anticipated, see Figure 8. The fitted Rayleigh pdf was then utilized to calculate the threshold gain, which in turn was multiplied by the envelope time series.

Again, the envelope was accumulated, but only for values over the chosen threshold according to the filtering algorithm. The result can be seen in Figure 9. Now the two major expected characteristics of the result can be seen, namely the material settling during the first part of the experiment, where the acoustic activity initially is high, but converges asymptotically towards a fixed value before there is a sudden increase towards the end of the experiment, after about 7200 seconds.

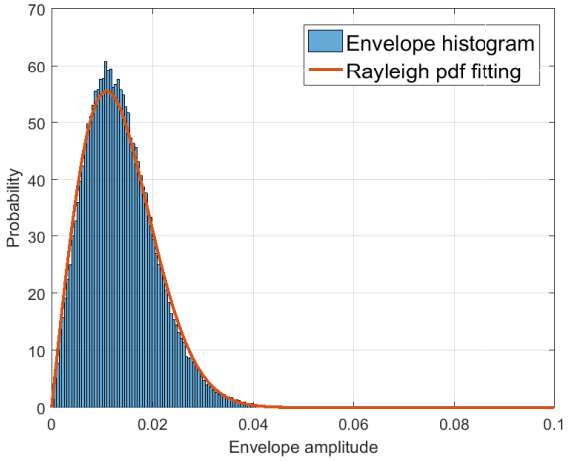

Figure 8. Histogram of AE envelope with Rayleigh pdf fit.

When zooming towards the end of the data set, see Figure 11, it can be seen that there is an event at 7100 seconds. Also, there was an increase in AE activity at about 6850 seconds. The extensometer data from this period is shown in Figure 10. Each point represents the maximum displacement in the displacement amplitude. It can be seen that about 100 seconds before final rupture, there is a sudden (exponential) ramp up of increase in elongation of the coupon, indicating crack initiation and its time evolution as seen in Figure 11.

The result indicates that the AE system detected crack initiation and propagation about 100 seconds before rupture of the coupon. Moreover, the AE also detected another incident about 250 seconds previous to this incident, which might be the first sign of the incipient fault. The fault is detected late in the test period, but due to the high intensity factor (stress) it is expected a very fast crack growth rate after initialization of the crack, as per the third regime of Paris law (Paris, Gomez, & Anderson, 1961). To automatize the detection process, a detection algorithm could be applied, e.g. (Moskvina & Zhigljavsky, 2003). For long cycle fatigue

To test the need of sampling frequency, the raw data was decimated. Good response in accumulated amplitude was achieved at a fifth of the sampling frequency (2 ksps), but was barely visible at a tenth of the sampling frequency (1 ksps), indicating the needed sampling requirement for such application. It should be noted that, due to such low sampling frequencies, the digitized data is to coarse in time for accurate source localization through multisensory detection.

5. CONCLUSION

The AE monitoring system presented in this research facilitates reduction of digital sampling and processing requirements for on-line monitoring of crack initiation and propagation for structural components due to cycling fatigue. Exper-

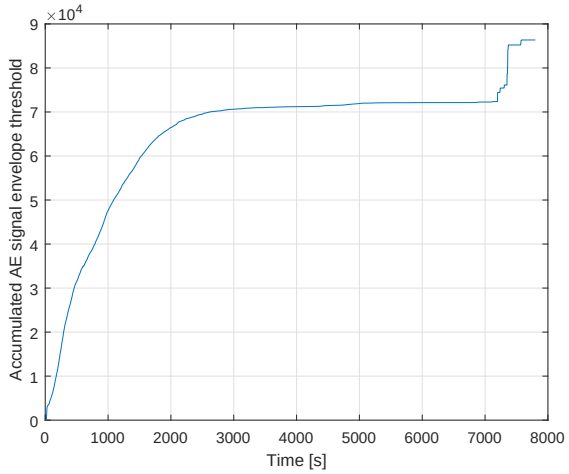

Figure 9. Time integration of filtered AE envelope signal.

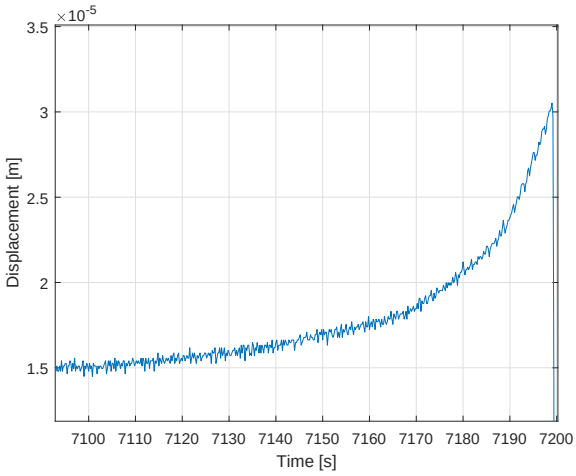

Figure 10. Amplitude of the extensometer evolving over time from crack initiation to rupture, where each point represent the max amplitude over one period.

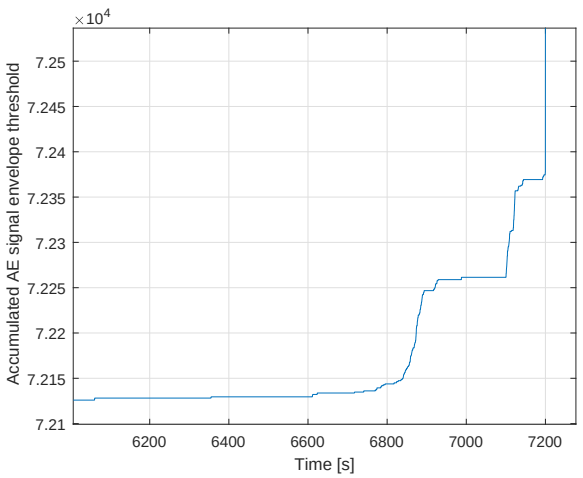

Figure 11. Time integration of filtered AE envelope signal over a shorter time period.

imental result indicated sensitivity to crack growth through correlation with extensometer measurements from the test coupon. In future work, the system will be tested for wire break detection on steel wire ropes during tension and bending cycle fatigue. Moreover, a physical failure model based on information received from the monitoring system that can be used to determine remaining useful life (RUL) of the steel wire rope will be developed.

ACKNOWLEDGMENT

The research presented in this paper has received funding from the Norwegian Research Council, SFI Offshore Mechatronics, project number 237896.

REFERENCES

Bechhoefer, E., Qu, Y., Zhu, J., & He, D. (2013). Signal processing techniques to improve an acoustic emissions sensor. In *Proceedings of the annual conference of prognostics and health management society.*

Berkovits, A., & Fang, D. (1995). Study of fatigue crack characteristics by acoustic emission. *Engineering Fracture Mechanics*, *51*(3), 401 - 416.

Drummond, G., Watson, J. F., & Acarnley, P. P. (2007). Acoustic emission from wire ropes during proof load and fatigue testing. *NDT&E International*, *40*, 94-101.

Grosse, C. U., & Ohtsu, M. (Eds.). (2008). *Acoustic emission testing*. Springer.

ISO. (2003). *Metallic materials – fatigue testing – axial-strain-controlled method* (No. 12106:2003).

Lindley, T. C., Palmer, I. G., & Richards, C. E. (1978). Acoustic emission monitoring of fatigue crack growth. *Materials Science and Engineering*, *32*(1), 1 - 15.

Liptai, R. G., Dunegan, H. L., & Tatro, C. A. (1969). Acoustic emissions generated during phase transformation in metals and alloys. *International Journal of Nondestructive Testing*, *1*, 213-221.

Mizutani, Y. (Ed.). (2016). *Practical acoustic emission testing*. The Japanese Society for Non-Destructive Inspection, Springer.

Moskvina, V., & Zhigljavsky, A. (2003). An algorithm based on singular spectrum analysis for change-point detection. *Communications in statistics. Simulation and computation*, *32*(2), 319-352.

Paris, P. C., Gomez, M. P., & Anderson, W. E. (1961). A rational analyic theory of fatigue. *The Trend in Engineering*, *13*(1), 9-14.

Roberts, T. M., & Talebzadeh, M. (2003). Acoustic emission monitoring of fatigue crack propagation. *Journal of Constructional Steel Research*, *59*(6), 695 - 712.

Van Hecke, B. E. (2015). *Development of novel acoustic emission based methodology and tools for bearing fault diagnostics* (Unpublished doctoral dissertation). University of Illinois at Chicago.

Yahr, G. T. (1993). *Fatigue design curves for 6061-T6 aluminum* (Tech. Rep.). Oak Ridge National Laboratory.

BIOGRAPHIES

Rune Schlanbusch received his MSc in Space Technology from Narvik University College (NUC), Norway in 2007, and a PhD in Engineering Cybernetics from NTNU, Norway in 2012. He currently holds positions as Senior Researcher at Teknova, Norway and II Associate Professor at Department of Technology, NUC. His major research interests include nonlinear control theory and stability analysis, Multiphysics modeling and simulation, intelligent sensor technologies and condition monitoring. He is currently a member of the IEEE control system society since 2008.

Eric Bechhoefer is the president of GPMS, Inc., a company focused on the development of low-cost condition monitoring systems. Dr. Bechhoefer is the author of over 100+ juried papers on condition monitoring and prognostics health management, and holds 23 patents in the field of CBM.

Thomas J. J. Meyer holds a BSc (Hons) in instrumentation systems from Sheffield Hallam University (UK) a License in physical and chemical measurements technologies from the University of Bordeaux (France) and a PhD, graduated in 2009, in solar cell physics from the University of Southampton (UK). He currently holds a business developer manager position at the research institute entitled Teknova (Norway) and an associate professor position at the department of engineering at the University of Agder (Norway).